EPJ Photovoltaics **15**, 15 (2024)

https://doi.org/10.1051/epjpv/2024009

Available online at:
www.epj-pv.org

Special Issue on 'EU PVSEC 2023: State of the Art and Developments in Photovoltaics', edited by Robert Kenny and João Serra

ORIGINAL ARTICLE OPEN ACCESS

Application of nowcasting to reduce the impact of irradiance ramps on PV power plants

Jonas Schaible[1,5,*], Bijan Nouri[2,**], Lars Höpken[2,4], Tim Kotzab[3], Matthias Loevenich[3], Niklas Blum[2], Annette Hammer[4], Jonas Stührenberg[4], Klaus Jäger[1,5], Christiane Becker[1], and Stefan Wilbert[2]

[1] Helmholtz-Zentrum Berlin für Materialien und Energie GmbH, Department of Optics for Solar Energy, 12489 Berlin, Germany
[2] German Aerospace Center (DLR), Institute of Solar Research, 04001 Almería, Spain
[3] German Aerospace Center (DLR), Institute of Solar Research, 70563 Stuttgart, Germany
[4] German Aerospace Center (DLR), Institute of Networked Energy Systems, 26129 Oldenburg, Germany
[5] Zuse Institute Berlin, Computational Nano Optics, 14195 Berlin, Germany

Received: 1 September 2023 / Accepted: 29 January 2024

Abstract. Short-term fluctuations in photovoltaic power plants, known as *ramps* and caused by clouds, challenge grid stability and efficient energy use. These issues are traditionally managed with battery energy storage systems, which, while effective, are expensive. We propose an alternative solution: the use of short-term irradiance forecasts, or *nowcasts*. Using a photovoltaic power plant in Germany and its simulated model, we demonstrated that nowcasts could cut ramp rate violations by 81%. This led to a reduction in required battery capacity by 71% and the required maximum battery power provided by 48%, at the cost of a 13% curtailment loss, i.e. loss through reduction of power. Our data set of 18 chosen days from 2020 with high variability conditions was scaled up to a year for the economic analysis. From an economic standpoint, nowcasts could lower the Levelized Cost of Electricity by 5.5% from 4.74 to 4.48 EUR cents, and even by 35% to 3.09 EUR cents with ideal forecasting, showing its potential. While nowcasts cannot completely replace batteries, they substantially reduce the need for such storage solutions. This results in cost savings and adherence to grid stability requirements, making nowcasts a complement or partial alternative to battery systems for mitigating power fluctuations in photovoltaic power plants.

Keywords: Nowcasting / ramp rate control / battery-less / active power curtailment

1 Introduction

The Sixth Assessment Report of the Intergovernmental Panel on Climate Change states, that 'without a strengthening of policies beyond those that are implemented by the end of 2020, [greenhouse gas] emissions are projected to rise beyond 2025, leading to a median global warming of 3.2 [2.2 to 3.5] °C by 2100' [1].

Fortunately, solar and wind energy offer substantial potential to reduce net emissions at low cost [1]. Solar power generation is subject to power fluctuations caused by the change in solar irradiance (e.g. bypassing clouds). Large irradiance fluctuations (now called ramps) result in large gradients of power generation (i.e. large ramp rates). The integration of variable renewable energy (VRE) sources challenges the reliability and stability of the electrical grid [2,3]. This is especially important for small islands or remote areas with a low grid-interconnection capacity [4,5] and large electrical grids with an annual VRE energy share of more than 15% [6]. Smoothing VRE fluctuations provides a solution for their further integration, but the photovoltaic system must be managed accordingly. As a consequence, grid operators can impose limitations on the variability of VRE sources via grid codes. An overview of the grid codes for different countries is shown in Table 1. Typically, so called battery energy storage systems (BESS) are proposed as a solution for output power smoothing but increase operating and investment costs [7]. Very short-term solar irradiance forecasting (nowcasting) has been studied as another solution to smooth VRE generation [8]. Nowcasting has the potential to reduce the required capacity and thus the costs of a BESS [9].

The literature review of Samu et al. [8] states that nowcasting tools in microgrid operations are still rare but their potential to provide ramp rate control is acknowledged. Three common methods for ground-based short term nowcasting are sensor networks, all-sky-imager-based

* e-mail: jonas.schaible@helmholtz-berlin.de
** e-mail: bijan.nouri@dlr.de

Table 1. Overview of regulations in different grid codes.

Country	Active power management	Ramp rate limit	Penalties
Australia	Required, except VRE [10, 11]	Western Power: ±max (10 MW/min, 15%/min) except VRE [12]; Horizon: ±15%/min including VRE [13] (low voltage: [14])	"causer pays" for frequency control, factors recalculated every four weeks based on historical data [15,16]
China	Required, including forecasts [17]	± 10%/min [17]	–
Denmark	Required [18]	± 100 KW/s [18]	–
Ethopia	Required [19]	–10%/min [19]	–
Germany	Required [20, 21]	0.33 %/s < r < 0.66%/s (after recieving instruction) [20]	–
Hawaii	–	±2 MW/min, ±1MW/s [22]	–
India	Required [23]	±10%/min [23]	–
Ireland	Required [24]	+30MW/min 22	–
Malaysia	Required [25]	±15%/min [26]	–
Puerto Rico	Required [22,27]	±10%/min [22,27]	Curtailment depending on compliance rate on a weekly basis [28]

tools, and various data-driven methods. Ground-based sensor networks consist of sensors distributed around the photovoltaic power plant (PVPP). Through coupling temporal and spatial information the power generation is estimated and ramp events can be detected. Typically, the prediction horizon is within several minutes with a high temporal resolution [29]. The nowcast horizon depends on the dimensions of the ground-based sensor network and the cloud movement speed. This can lead to an extensive required network size [30]. All-sky-imager-based tools can either be used by statistical models or physical models. All sky imager take full hemispheric pictures of the sky. Saleh et al. introduced a physical model based on cloud-motion detection via sky images to smooth PV output power [31]. The method supports the feasibility of battery-less smoothing. The nowcast accuracy influences the number of missed ramp rate events and curtailed energy and is thus critical for the adaptation as a proactive smoothing approach. Paletta et al. studied deep learning irradiance nowcasting models from sky images [32]. Current modeling approaches suffer from uncertainties regarding correct spatial and temporal cloud movement and their interaction with irradiance [33]. Data-driven methods provide promising improvements by following the trend of persistence models and reducing the impact of the most extreme errors. However, they often miss accurate predictions of ramp events [32]. An exemplary study of deep-learning-based solar nowcasting for power smoothing using all sky images shows improvements [33]. An extensive analysis of the potential of nowcasting in reducing the costs of energy in PV plants under ramp-rate restrictions was performed by Círes et al. [9]. Hereby, the battery-less control strategy resulted to be the most cost-effective solution under the conditions of the study. However, the potential of nowcasting was estimated by using ideal nowcast without uncertainties. To quantify the realistic potential, these must be estimated by using realistic nowcasts with uncertainties in ramp detection.

According to [34] the importance for the field to advance is to come from solar irradiance forecasting to PV power forecasting, which is part of the motivation for this study. Our parametric approach, based on probabilistic forecasting, utilizes state-of-the-art all-sky-image-based nowcasting with taking into account the uncertainties of each time step for predictive active power control. From the system operators view it is of interest to estimate the required BESS capacity and BESS power for control purposes since it will reduce overall system investment following [7,10]. Liu and Du presented in their review on the evolution towards dispatchable PV a road map for future studies and their motivation [35]. They identified PV forecasting, energy storage, and inverter-controlled curtailment as the relevant technologies to eliminate uncertainty and variability for the goal of dispatchable PV. The estimation of the achievable level of control requires further work to be generalized for differently scaled PVPP. In this study, the level of control is estimated and its economic impact is studied.

This study is about the application of a state-of-the-art all-sky-image-based nowcasting model for PVPP ramp rate control. Special focus lies on the effect of uncertainties on the ramp rate control. Hereby, a large PVPP is simulated and validated by the energy production data of that PVPP. A control strategy with and without BESS is developed and estimates for a battery capacity reduction are given. As an example, this study will provide a case for nowcasting-based ramp rate reduction. The novelty in this study is the combination of the application of all-sky-imager based nowcasting for power smoothing in a realistic case with validation data, the study of the nowcasts uncertainties for

Table 2. Dictionary for terms used with regard to the simulation and control strategy.

Output power	Simulated power provided by the PVPP without contribution of battery
System power	Simulated power provided by the PVPP with contribution of battery and control strategy
Validation power	Real total power production data of PVPP
Dump power	Power provided or drawn by the BESS to reach aimed SOC
Ramp	Event, where two succeeding time steps or lead times have a power gradient greater then the ramp rate limit
Ramp depth	Absolute power value of second time step or lead time in ramp
Ramp height	Absolute power value allowed at current time step under ramp rate limit

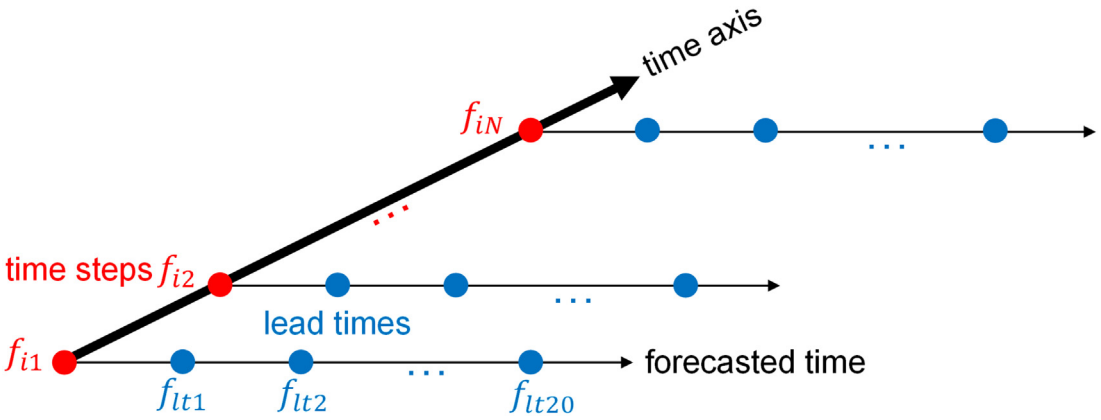

Fig. 1. Temporal resolution of the nowcasting system: the nowcast instances are updated in time steps of 30 s. For each instance, a nowcast with a horizon of 20 min is given in a 1 min resolution resulting in 20 lead times.

the control strategy and the estimation of a possible reduction in required battery capacity and battery power. Further, the economic potential was quantified and areas of future research defined.

2 Simulation details

To study the research question, a modeling approach is chosen. The model of a utility-scale PVPP is proposed and integrated into a simulation environment. Thereby, the nowcasts are turned into output power predictions. Further, a model for a BESS is integrated. The control strategy then enforces the system power to comply with the grid code. Table 2 shows the terms used with regard to the simulation and control strategy.

2.1 Nowcasting system for solar irradiance

The nowcasting was performed with a subset of 13 all sky imagers of the Eye2Sky measurement network operated by German Aerospace Center (DLR). The subset covers an area of 13×12 km^2. The configuration and method are described in detail in [36]. The results of the nowcast approach are irradiance maps covering an area of up to 156 km^2 with a spatial resolution of 50 m and a prediction horizon of 20 min ahead. The respective time of the measurement is called time step. Nowcasts are created in one-min steps, called lead times. Thus, leading to twenty predictions (lead times) per time step. Further, the measurement at the time step adds a 21st irradiance map. Every time step results thus into 21 irradiance maps. In the course of the day, the interval between two sets of nowcasts (i.e. time step) is 30 s. Figure 1 shows the schematics of the nowcasts. The final products of the nowcasts include direct normal irradiance (DNI), diffuse horizontal irradiance (DHI), and global horizontal irradiance (GHI) at the PVPP site under study. Reference [37] describes the procedure to obtain global tilted irradiance (GTI).

Solar irradiance nowcasts are subject to uncertainties. The magnitude of these uncertainties is dependent on the prevailing variability of the solar irradiance. To quantify the degree of variability, a classification method of the sky conditions based on Schroedter-Homscheidt et al. [38] and adapted by Nouri et al. [39] is applied to the nowcasts. In Table 3, the variability classes and sky conditions are displayed. A class for every time step is derived from 13 distinct variability indices over a 15-min time window of irradiance conditions. Historical observations and nowcasts are combined for this study. This makes it possible to classify the irradiance conditions of the lead times as well. For example, the classification of a lead time 10 nowcast uses the corresponding 5 min of historical data and the lead times 1–10 min ahead. Nouri et al. [40,41] developed a method to create probabilistic nowcasts from deterministic nowcasts. This method is applied in this work to create a probabilistic nowcasts from the irradiance maps provided by the all sky imager network. Each percentile of the

Table 3. Description of DNI-variability classes based on Schroedter-Homscheidt et al. [38] and Nouri et al. [39]. Each DNI variability class indicates a certain sky condition and a specific level of variability.

Class	Sky conditions	Variability
1	Mostly clear sky	Low
2	Almost clear sky	Low
3	Almost clear sky	Intermediate
4	Partly cloudy	High
5	Partly cloudy	Intermediate
6	Partly cloudy	High
7	Almost overcast	Intermediate
8	Mostly overcast	Low

probabilistic nowcasts describes a value below which future irradiance is expected with respective probability. Thus, a pair of percentiles encloses a corresponding prediction interval. Just as for deterministic nowcasts, the probabilistic nowcasts produce solar irradiance maps with lead times of up to 20 min. The control strategy for the PVPP is based on the probabilistic nowcasts.

2.2 Datasets

The following datasets were used in this study: From year 2020, nowcasts for 18 days with a variety of irradiance conditions such as clear-sky days as well as days of highly variable conditions are used for a Location in Northern Germany. Figure 2 shows the number of time steps and the distribution of classes per day on the left and on the right the relative frequency of classes for the whole year at the PVPP's site. Aside from the dominant class 8 with low variability, the dataset includes large fractions of intermediate and high variability classes. The days are chosen with regard to the development of the control strategy and includes largely challenging days. I.e. fast and large changes of irradiance, days with all classes represented and days with large cloud coverage. This dataset is used for the control strategy. The PVPP at this location a nameplate power of 20.8 MWp. From this PVPP and for these 18 days, the respective dataset of the photovoltaic production at inverter level in one-min resolution is available as a validation dataset, which is used for validation of the PVPP model. The following data management operations were performed. The datasets were required to cover the whole day of operation. Days not satisfying this constraint were not selected, resulting in the 18-day dataset. A systematic time shift by a few minutes for all days was observed for a low fraction of inverters. These shifts were corrected to the timestamps of neighbouring inverters, matching the timestamps of the vast majority of inverters. Lastly, nonphysical values, such as negative values, were omitted and filled with the preceding values. Further, a dataset with DNI-classification is available for the whole year 2020 and was used for up-scaling the results as described in Section 4.2.

2.3 Energy yield simulation engine

The energy yield (EY) was calcualated with the tool Yield Assessment Calculation and Optimization Program (YACOP), which is developed by the DLR [42]. YACOP is a simulation framework for the yield assessment and design of energy conversion systems and can be used to simulate solar energy systems following the 'SolarPACES Guideline for Bankable STE Yield Assessment [43]'. It is intended to work with quasi-static and quasi-dynamic power plant models to estimate the EY over a given time series. Here, quasi-static refers to the description of dynamic processes as a time series of operating points with intervals (time steps) 30 s to 60 min [44]. Quasi-dynamic refers to simplified models to describe dynamics. During one iteration all inputs are assumed to be constant. Therefore, the dynamics of the power generation are limited to the resolution of the time steps. For this work, YACOP was extended to process spatially-resolved nowcasts.

2.4 Photovoltaic system model

A common approach to model a PVPP is to divide the model into smaller, independent models. The pvlib python [44,45] is a library for implementing PV system models. It is based on the pvlib Matlab toolbox which is developed and maintained at Sandia National Laboratories [46]. The following quantities are calculated with models from pvlib python:

- The angle of incidence (AOI), as the angle between the solar vector and the surface normal.
- The relative airmass at sea level and absolute (pressure-adjusted) airmass. In this context, the airmass is a measure of the relative path length through air that a direct beam from the sun travels until it reaches the PV module. It is dependent on the apparent sun angle and pressure.
- The effective irradiance, the five parameter values for the single diode model, and the single diode model that solves the single diode equation to obtain the current-voltage curve (IV curve), as well as the maximum power (using Sandia Array Performance Model (SAPM)).
- The cell temperature calculation (SAPM cell).
- The azimuth and sun height angle of the sun (NREL−Solar Position and Intensity (SOLPOS) model [47]).

The following sections describe the calculation methodology along the five modeling units Irradiance Analysis, Array, Inverter, Output Power Control and Energy Storage.

2.4.1 Irradiance analysis

The nowcasting output is treated as follows: For every nowcast instance a data structure is set up containing the complete DNI and GTI irradiance maps for all lead times (21×) and percentiles (9×), as well as the DNI variability classes. The selection of the required inputs can be controlled via seven parameters, which are time step(s), lead time(s), relative coordinates of the irradiance map and the irradiance value(s) (DNI, GTI) of the respective percentile(s). For this study, the sizes of the DNI and GTI

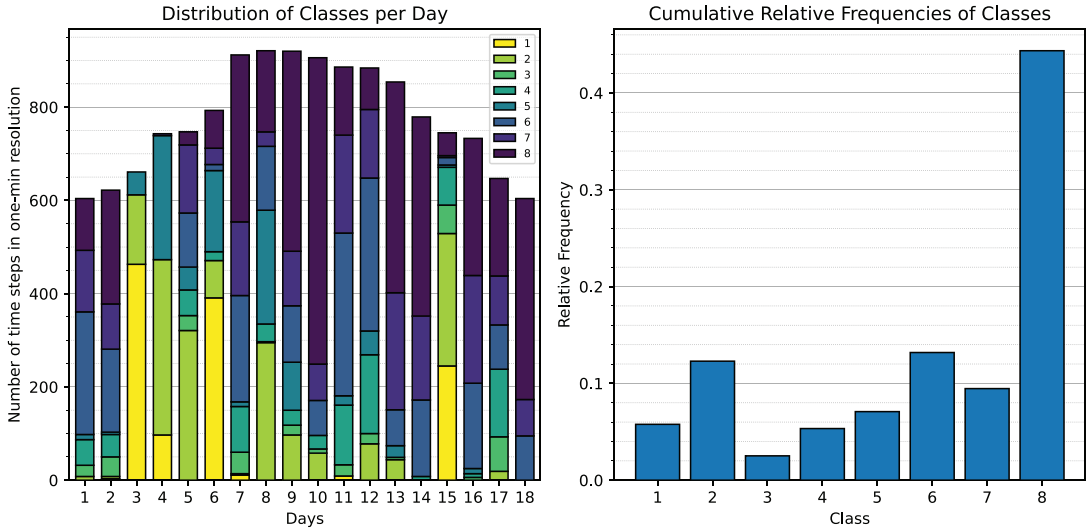

Fig. 2. Left: the distribution of classes for the 18 example days. These range from days with classes 1 or 8 being dominant to days with less dominant classes. Right: cumulative relative frequency of the variability classes of year 2020. The most dominant class at the PVPP's site is class 8 being mostly overcast.

irradiance maps are reduced to only include the positions of the PVPP arrays. Only the current time step is passed through the simulation during one iteration. Because the uncertainty of nowcasts increases with the lead time [48], a limited number of lead times is processed during each time step. The largest ramp observed in the GTI dataset of the year 2020 is 65%. With an assumed ramp rate limit of maximum 10% change in PV-system power per minute, a ramp of 65% magnitude would need to be detected 7 min in advance (lead time 7) in the case of ideal nowcasts. Since nowcasts are subject to uncertainties, for redundancy, lead times up to lead time 10 are included. Finally, a percentile is chosen depending on the control strategy (see Sect. 3). This can be either a single percentile for the duration of the simulation, or the percentile is chosen individually for each time step and lead time based on the prevailing DNI variability classes.

2.4.2 PV array

The calculation of the direct current power (P_{DC}) per array largely follows the Sandia Photovoltaic Array Performance Model (SAPM), introduced by King, Boysen, and Kratochvil [49]. The parameters, f. e. soiling loss, were studied by Blum [50] for the exact power plant.

The model accounts for the major influences on the performance. These are given by the meteorological conditions, as the irradiance (GTI and DNI per array), the ambient temperature, the wind speed at height of 10 m, and the air pressure. Depending on the available power plant information, a large set of PVPP-specific parameters can be defined, namely, the sites location information (longitude, latitude, height), the timezone of the simulation, the orientation of the PV modules (azimuth, elevation), the PV-module specifications, the array configuration (number of modules per string, number of strings per inverter), and the loss factors (DC wiring correction, mismatch correction, module degradation, soiling losses, AC wiring correction). The above-mentioned SAPM model outline is displayed in Figure 3. The first step in the SAPM model is the calculation of the effective irradiance E_e via the optical model. The direct irradiance is obtained from DNI by considering the AOI. The diffuse irradiance is the GTI minus the obtained direct irradiance. The AOI results from the time, location, and orientation of the power plant, and the airmass from solar elevation angle and pressure. The parameters F_1 and F_2 account for the spectral and reflective losses of multi-crystalline silicon PV cells with a glass module cover without anti-reflective coating.

The cell temperature T_c is estimated via the E_e-induced electrical losses, the wind speed WS, and the ambient temperature T_{amb}. The empirical constants a and b depend on the environment of the PVPP installation. Here, the values for a green-field open-rack PV installation are used. $\Delta T/E_0$ refers to the temperature difference between the module backside and the PV cells under standard test conditions E_0.

By combining the E_e, T_c, and parameters specific to the PV module type the five parameters shunt resistance, series resistance, light-generated current, diode saturation current, and modified diode ideality factor are determined according to [51]. These five parameters solve the single diode equation, which approximates the PV module by an electrical circuit of a current source, a diode, a serial, and a shunt resistor. The direct current power per module ($P_{\mathrm{DC,m}}$) is then obtained from the resulting current-over-voltage (I-V) curve of the single diode model.

The last step is the application of the array configuration. Thereby, the module outputs are combined (N_m,N_s) and multiplied by the DC loss factor. The result is the DC power per string $P_{\mathrm{DC,a}}$.

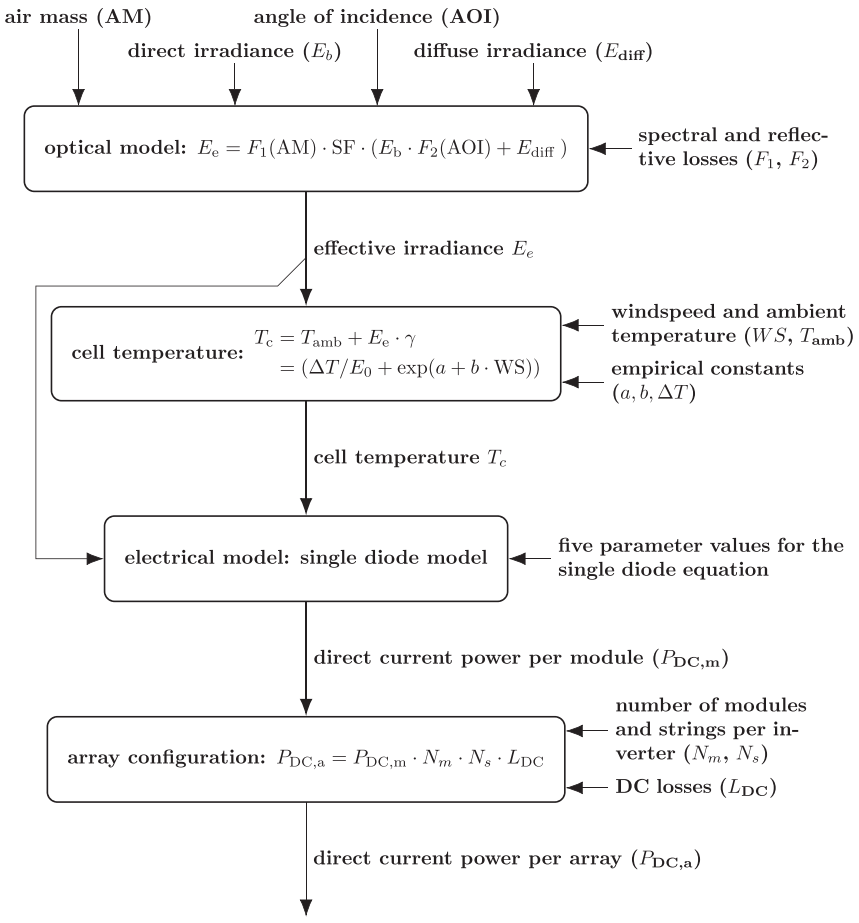

Fig. 3. Flowchart of the photovoltaic array model including the optical, cell temperature and electrical model, the array configuration, and the respective inputs and parameters. The modelling unit largely follows the Sandia Photovoltaic Array Performance Model (SAPM), which was introduced by King, Boysen, and Kratochvil [30].

2.4.3 Inverter

The efficiency of common DC to alternating current (AC) power inverters is approximately constant for capacities above 10% of the designed capacity. For values below that threshold, the efficiency quickly approaches zero and must be considered for low irradiance conditions, which occur regularly at the PVPP sites location.

$$P_{\text{DC0}} = P_{\text{AC0}}/\eta_{\text{nom}}, \tag{1}$$

$$\zeta = P_{\text{DC,a}}/P_{\text{DC0}}, \tag{2}$$

$$\eta = \eta_{\text{nom}}/0.967 \times (0.9858 - 0.0162 * \zeta - 0.0059/\zeta), \tag{3}$$

$$P_{\text{AC,a}} = \min\left(\eta P_{\text{DC,a}}, P_{\text{AC0}}\right). \tag{4}$$

The PV-Watts inverter model from [52] considers this behavior and requires only two parameters (nominal efficiency (η_{nom}), nominal AC power (P_{AC0})) besides the $P_{\text{DC,a}}$. Equations (1) to (4) determine the $P_{\text{AC,a}}$. Finally, the $P_{\text{AC,a}}$ of all arrays of the power plant are combined with the AC power of the PVPP P_{AC}.

2.4.4 Energy storage

A simple energy storage model is integrated, which was developed at DLR [42]. It accumulates the charge (discharge) energy and provides the energy content and state-of-charge (SOC). Further, the round-turn efficiency and the maximum charge and discharge power are considered. In every time step, the parameters charge power, discharge power and previous energy content are set. The model compares the proposed charge and discharge power to the current energy content of the battery. If the battery cannot absorb or provide the proposed charge and discharge power for the duration of one time step, it sets the respective limits. The model applies the round-turn efficiency factor to the charge power, set to 86%. Thus, the energy stored in the battery is fully retrievable without further losses. The nominal capacity of the battery storage is subject to the control strategy and results and will be discussed in Section 5. The largest gradient of the GTI within 1 min resolution which appears in the measurement data for the whole year 2020 was 65%. Based on this, the maximum required power of 13.5 MW is set, which is 65% of the 20.8 MW rated power of the PVPP. Following the worst fluctuation model for battery capacity estimation of Marcos et al. [53], described

Table 4. Parameters PV model.

Origin	Parameter name	Parameter value
PVPP site	Time zone	UTC+0
	Max power plant	20776000 [W]
PV module	Module power	265 [W]
	Modules per string	40
	String per inverter	2
	Inverter systems	980
Simulated battery	Max battery power	13527877 [W]
	Battery capacity	2591806 [Wh]
	Battery round-trip efficiency	0.86
Correction factors	Dc wiring correction	0.985
	Mismatch correction	0.99
	Module derate correction	0.9948
	Soiling factor	0.98
Inverter	Nominal inverter efficiency	0.987
	AC wiring correction	0.98
Simulation settings	Time step	1 [min]
	SOC at start	50 [%]
	Percentile strategy	MIX
	Lead times	10 [min]
	Max dump power	0.08 [% of max PVPP power]

by equations (5) and (6), the minimum battery capacity for the benchmark case with battery smoothing is 2.6 MWh.

$$C_{\mathrm{BAT}} = 2{\cdot}E_{\mathrm{BAT,MAX}} = \frac{1.8{\cdot}P_{\mathrm{MAX}}}{3600}\left[\frac{90}{2{\cdot}r_{\mathrm{MAX}}} - \tau\right], \quad (5)$$

$$\tau = a{\cdot}l + b \,\text{with}\, a = 0.042\,(\mathrm{m/s})\,\text{and}\, b = -0.5\,\mathrm{s}. \quad (6)$$

Here, C_{BAT} is the battery capacity, $E_{\mathrm{BAT,MAX}}$ is the maximum energy the battery has to provide, P_{MAX} is the rated power of the PVPP, and r_{MAX} is the maximum allowable ramp rate [%/s]. Further, τ is a time constant empirically correlated to l [s], the shortest length of the PVPP site.

2.4.5 Output power control

The modelling unit Output Power Control contains the ramp rate control strategy as described in Section 3. It is connected to the Inverters and Energy Storage and manages the system power. The control strategy provides setpoints of operation for the PVPP. The realization of the setpoints (i.e. settling time) is assumed to be instantaneous, but in reality, is achieved within seconds [54]. Therefore, the inverter is assumed to deviate from the maximum power point tracking (MPPT) algorithm and to operate at lower power. This effect is neglected here, since the time resolution of interest is 1 min, which is an order of magnitude greater than the settling time of typical inverters. Table 4 includes all parameters which remain constant during the simulation. Since the grid code of Germany is based on instructions, the grid code chosen for this study is a maximum of 10% of rated power per minute.

3 Control strategies

This section contains the control strategy of an example grid code that limits the maximum allowed fluctuation in power generation to 10% rated power per minute [55]. Every time step that does not meet this requirement counts as ramp. The respective depth of a ramp is quantified as a percentage of the rated power. To comply with the grid code, a hybrid control strategy based on the projected output power of the PVPP (nowcast strategy) and SOC of the battery (battery strategy) is implemented. The battery strategy is based on [5,56]. The nowcast strategy provides information about the occurrence and depth of future fluctuations and the resulting upper limit for system power.

3.1 Strategy for ramp detection

The section describes the selection of the percentile used for ramp detection and the ramp detection itself. In the strategy (called: MIX), the resulting classes of each lead time determine the percentile for the respective time step. This results in a collection of classes per time step equal to the number of lead times. From that collection, the percentile, under which the simulation is operating at this time step, is chosen according to Table 5. Here, the occurrence of different classes in the collection, in combination with the irradiance variability classes define the resulting percentile (Tab. 6).

Figure 5 shows the output power of time step 11:50 of March 16th, 2020. The percentile 50 curve (black) behaves similarly to the deterministic output power for the 20 min ahead (11:51 until 12:10). The grey-scaled areas are the respective prediction intervals (20%, 40%, 60%, 80%) for

Table 5. Selection of percentile based on the variability class and the number of different classes per time step (occurrence).

Percentile	Classes	Occurrence
P50	1,2,8	One class
P40	1,2,8	Two classes
P30	3,5,7	One class
P20	3,5,7	Two classes
P10	4,6	One / two classes
P10	1 to 8	Three or more classes

Table 6. Overview of ramps passed on to the control strategy for time step 11:50.

Time occurrence	Current lead time [min]	Power [MWh] Ramp depth	Ramp height
11:51	1	3.60	5.68
11:55	5	3.65	14.04
11:58	8	3.62	20.24

the same time window. Percentile P10 was selected for (Fig. 5) according to Table 5. The red dashed lines show the deepest ramps for each time step in the nowcast horizon, that is up to lead time 10 (12:00). The lines start at the respective maximum output power possible under the ramp rate limit (referred to as ramp height) and evolve in 10% rated power steps down to the predicted ramp depth. Thus, the ramps end at the predicted power value of percentile P10 at the time of occurrence (e.g in Fig. 5: 11:51 (lead time 1), 11:55 (lead time 5), and 11:58 (lead time 8)). The predicted output power is scanned for ramps in each iteration of the simulation (time step). For each detected ramp, occurrence time and depth are compared to previously detected ramps. The deepest ramps per occurrence time are stored until the time step passed.

3.2 Nowcast strategy

The goal of the nowcast strategy is to limit the output power with regard to detected ramps. Figure 4 shows the schematics of the nowcast strategy, whereas Figure 5 shows an example of the strategy.

The first step of the nowcast strategy is the selection of detected ramps. The parameters of this selection process are the number of ramps per occurrence time and the number of neighboring occurrence times which observed a ramp. The default selection parameter is that a ramp must at least be observed two times. Either two times in the same occurrence time or distributed over two neighboring occurrence times. As the second step, the minimum ramp height and nominal power are passed on as output power. Next, two limits are applied: the first limits the gradient between the output power of the previous time step to the constraint. The second checks if the power plant can provide the proposed output power. If not, the output power is set to the available power (validation power). Finally, the output power is determined. When the output power is larger than the validation power (fourth step in Fig. 4), the gradient can exceed the limits. This will result in a breach of the ramp rate constraint, if no battery is installed. An ideal nowcast would provide the exact ramp depth and ramp height and thus no breaches would be observed.

As an example, Figure 5 shows the validation and the output power from time step 11:50 to 12:00 as well as the ramp-up limitations for the output power. At time step 11:50, the output power is limited to the ramp height (Tab. 6). At 11:51, the end of the ramp is reached. At 11:52 the output power is limited by the ramp rate constraint, but for the up ramp. At 11:53, the output power is limited by the validation power. Time steps 11:54 to 11:56 follow the same reasoning as 11:50 to 11:52. In 11:57, ramp height constraint beats the up ramp constraint and the output power is limited by the ramp height. Time steps 11:58 and 11:59 follow the same reasoning as 11:51 and 11:52. Finally, time step 12:00 is, again, limited by the ramp constraint. The case, which is not displayed in Figure 5 is when validation power is lower than the output power. In these cases, the ramp rate constraint can be breached when no backup power is available. For this reason, the battery strategy in the following section is set up. It can provide the necessary power to avoid breaching the constraint.

3.3 Battery strategy

The battery strategy has the purpose to smooth the output power of the PVPP to comply with the ramp rate constraint in case of a prediction error. Ideally, this additional power would be obsolete but since the uncertainty of the nowcast is non-zero and ramps can be missed, the battery provides the necessary security to comply with the ramp rate constraint.

The battery strategy is driven by the state of charge (SOC) and reacts to the output power. Figure 6 shows the schematics of the battery strategy. To avoid unnecessary (dis-)charge two constraints are checked at the start, namely whether the current time step projects ramps in lead time 1 or 0 and whether the output power was limited by the validation power. If not, the next two steps are skipped. If yes, the SOC is compared to the aimed level. If this level is not reached, the dump power is estimated and added or subtracted from the output power which leads to the proposed system power. The fourth step determines the gradient between the previous and the current system power. If the gradient exceeds the limits, the system power is set to be within the gradient limits. The corresponding charge and discharge power are then set concerning the available power (validation power). If the (dis-)charge power is not within the limits, it is corrected to the maximum (dis-)charge values the battery can provide. This could lead to a breach of the ramp rate constraint. Finally, the system power is determined. The proposed strategy MIX is compared to the strategy validation (VAL) and ideal validation (IDV). Strategy VAL has no

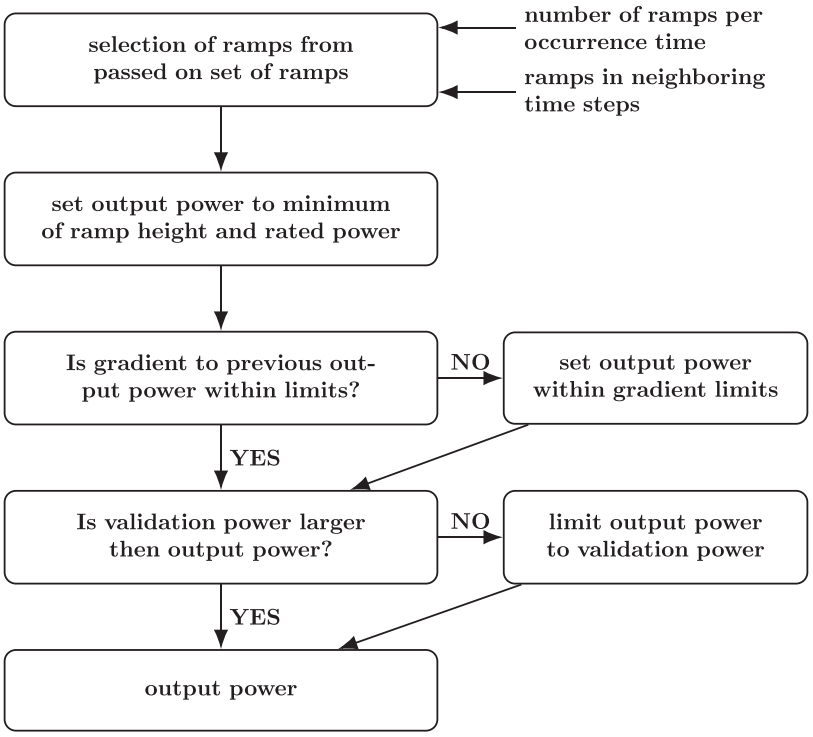

Fig. 4. Nowcast strategy to limit the output power to the ramp height, the gradient constraint, and the validation power.

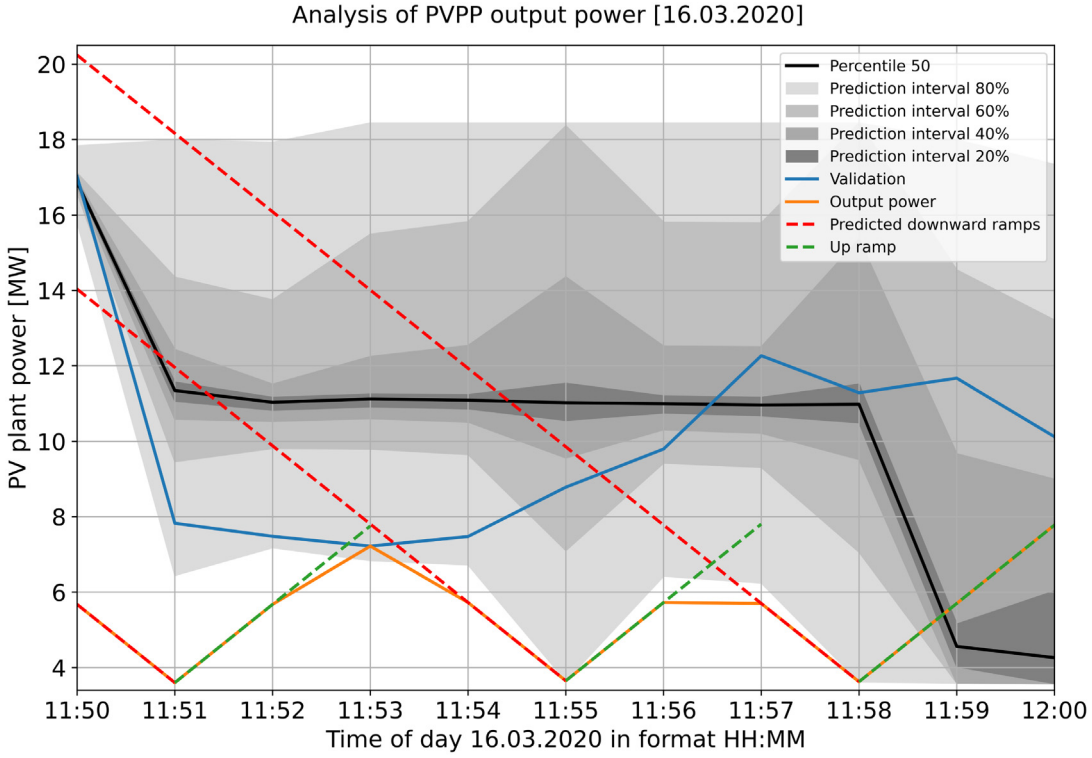

Fig. 5. Simulated and measured PVPP output power of 16.03.2020 at 11:50. Time steps 11:50 until 12:10 represent the predicted future values via the probabilistic nowcast (black and grey curves). The blue validation curve is obtained via measurements and is not part of the prediction.

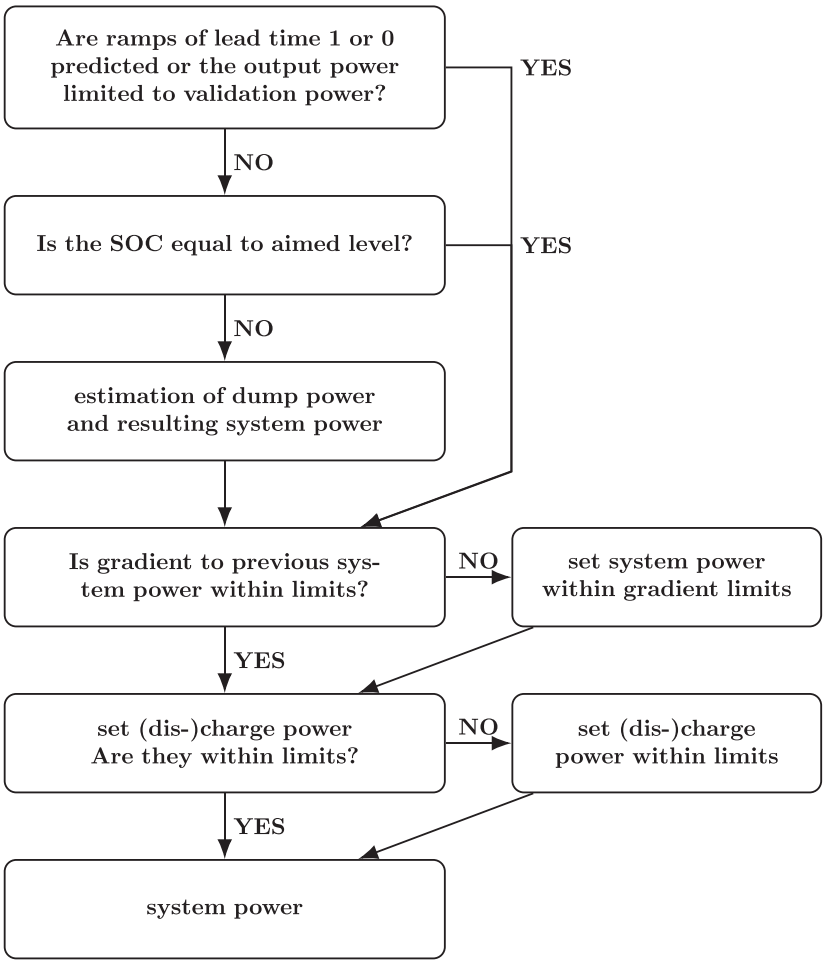

Fig. 6. Battery strategy to smooth the output power gradient and keep SOC at the desired level. The final power output of the hybrid system is the system power.

nowcasting and smoothes ramps via the BESS. Strategy IDV uses ideal nowcasts with no uncertainty. Thus, a battery storage for this strategy is not necessary.

4 Economic systems simulation

To estimate the economic consequences of the imposed grid code and the uncertainties of the nowcasts, an ecomonical analysis is performed, which is based on [57]. Here, the levelized cost of energy (LCOE) is the chosen figure of merit to allow comparisons between the strategies performance.

4.1 Costs of PV, battery and nowcast systems

The lifetime and costs of the PV system need to be defined for later use in the economic analysis (Sect. 5.2). The lifetime is set to 30 years according to [58] and [59]. The investment costs vary significantly depending on the country. While module prices are relatively similar, costs for the remaining hardware, installation and other soft costs like design and financing can be very different [60]. Considering this, the 2021 investment costs for Germany were taken as a baseline for a 2023 estimation using the forecasted cost evolution of the National Renewable Energy Laboratory (NREL) [61]. NREL expects the utility-scale PV cost to fall by roughly 7.9% from 2021 to 2023. Taking a currency conversion factor of 0.9 into account [62], equation (7) gives the final PV investment costs used for this analysis (values extracted from [60,61]).

$$\begin{aligned} \mathrm{CAPEX_{PV}} &= 694\,\frac{\mathrm{USD}}{\mathrm{KWp}}\cdot(1-0.079)\cdot 0.9\,\frac{\mathrm{EUR}}{\mathrm{USD}} \\ &= 575.26\,\frac{\mathrm{EUR}}{\mathrm{KWp}}. \end{aligned} \tag{7}$$

The operating costs for Germany are obtained by applying the United States NREL costs forecast. Equation (8) yields the final operating costs (values extracted from [40,42]).

$$\begin{aligned} \mathrm{OPEX_{PV}} &= 13.3\,\frac{\mathrm{EUR}}{\mathrm{KWp}\cdot a}\cdot(1-0.0585) \\ &= 12.52\,\frac{\mathrm{EUR}}{\mathrm{KWp}\cdot a}. \end{aligned} \tag{8}$$

Table 7. Battery CAPEX for different storage durations and powers in 2023. Green colored values taken from [66,67,68] in USD/KW and converted to EUR/KW. Blue colored values are extrapolated linear and magenta colored values are interpolated logarithmic.

	Storage duration [h]					
Storage power [KW]	0.5	1	2	4	6	8
600 (commercial)	847.42	929.64	1094.08	1422.95	1751.83	2080.71
13537.88	445.33	562.24	786.31	1217.58	3453.50	2058.21
60000 (utility scale)	327.41	442.08	671.43	1130.14	1588.84	2047.55

The required charge rate (CR) of the battery, defined in equation (9), is higher than the highest commercially available. The closest CR is 2, which means the battery can provide the power for a duration of 0.5 h.

$$CR = \frac{P_{\mathrm{PV,MAX}}}{C_{\mathrm{BAT,MAX}}} = 5.219. \tag{9}$$

Equation (10) shows the calculation of the required battery capacity of a 0.5-h storage system.

$$C_{\mathrm{BAT,0.5h}} = P_{\mathrm{BAT,MAX}} \cdot 0.5\,\mathrm{h} = 6763.94\,\mathrm{kWh}. \tag{10}$$

Since lifetime assessment of batteries is a highly complex topic [63] and accurate calculations, taking the specific utilisation into account, exceed the scope of this study, a simplified lifetime model is chosen. For this, a lifetime of 15 years is assumed in which no ageing takes place [59,64]. After these 15 years the battery system has to be replaced, costing another 30% of the initial investment [59]. The investment costs for both storages are extrapolated from [66,67] and [67], using the moderate scenario for 2023. The green values in Table 7 are extracted from the aforementioned sources and converted to Euro using a factor of 0.9. Using the fact that the prices appear to scale linearly with the storage duration, the missing values for shorter durations (higher C-rates) of the commercial and utility scale storage systems are extrapolated, and marked purple. Finally, since the size of the designed storage is between the two references, the prices are interpolated (magenta values). This time a logarithmic progression is assumed. Equations (11) and (12) show the interpolation of the CAPEX for the 1-h storage. The indexes *com* and *uti* refer to the commercial and utility scale reference storages respectively. Operating costs are assumed to be 2% of the CAPEX per year [59,68]

$$X = \log\left(\frac{P_{\mathrm{BAT,MAX}}}{P_{\mathrm{com}}}\right) \cdot \log\left(\frac{\mathrm{CAPEX}_{\mathrm{uti,1h}}}{\mathrm{CAPEX}_{\mathrm{com,1h}}}\right) / \log\left(\frac{P_{\mathrm{uti}}}{P_{\mathrm{com}}}\right) = -0.2184. \tag{11}$$

$$\mathrm{CAPEX}_{\mathrm{bat,1h}} = 10^{X} \cdot \mathrm{CAPEX}_{\mathrm{com,1h}} = 562.2\,\frac{\mathrm{EUR}}{\mathrm{KW}}. \tag{12}$$

For the nowcasting system solely the costs and lifetime are necessary for the economic analysis. The lifetime is set to 15 years which corresponds to the expected lifetime of the all sky imagers. Investment costs are estimated, considering the cameras, electrical equipment, a computer, installation and software costs. They amount to $CAPEX_{\mathrm{NC}}$ = 25000 EUR. It is assumed that the PV plant is already equipped with meteo stations and scaffolding to install the all sky imagers. Applying the same assumption as for the storage system, reinvestment costs after the end of the expected lifetime are set to 30% of the original costs [59]. During operation the cameras need frequent cleaning. To estimate the associated expenses, a technician™s labour costs for 10 min per day are used [69].

$$\mathrm{OPEX}_{\mathrm{NC}} = \frac{1}{6}\frac{h}{d} \cdot 365\,\frac{d}{a} \cdot 39.5\,\frac{\mathrm{EUR}}{\mathrm{h}} = 2402.92\,\frac{\mathrm{EUR}}{\mathrm{a}}. \tag{13}$$

4.2 Levelized cost of energy

The LCOE for any given configuration is determined according to equation (14) [70].

$$\mathrm{LCOE} = \left(I_0 + \sum_{\mathrm{t}=1}^{L_{\mathrm{PV}}} \frac{C_{\mathrm{sys,t}}}{(1+i)^t}\right) \Big/ \left(\sum_{\mathrm{t}=1}^{L_{\mathrm{PV}}} \frac{E_{\mathrm{sys,t}}}{(1+i)^t}\right). \tag{14}$$

As the name suggests, it is a measure for the costs involved in electricity production and depends on the technology used. It is calculated by dividing the overall lifetime costs by the total energy supplied and thus is usually presented in [ct / KWh]. The investment costs I_{o} contain the upfront costs of all parts of the system. Depending on the configuration these are PV, storage and/or nowcasting costs. They are calculated by multiplying the CAPEX of the respective system with its size. The second part of the numerator contains all costs that occur during operation. These are just the yearly operating costs of the systems for most of the years. However, since the storage and nowcasting systems have shorter lifetimes than the PV system, they need replacement at their end of life and these expenditures need to be considered in the year they arise in. Taking future cost reductions and reusability of parts of the installations into account, the reinvestment costs are assumed to be 30% of the original costs [40]. The

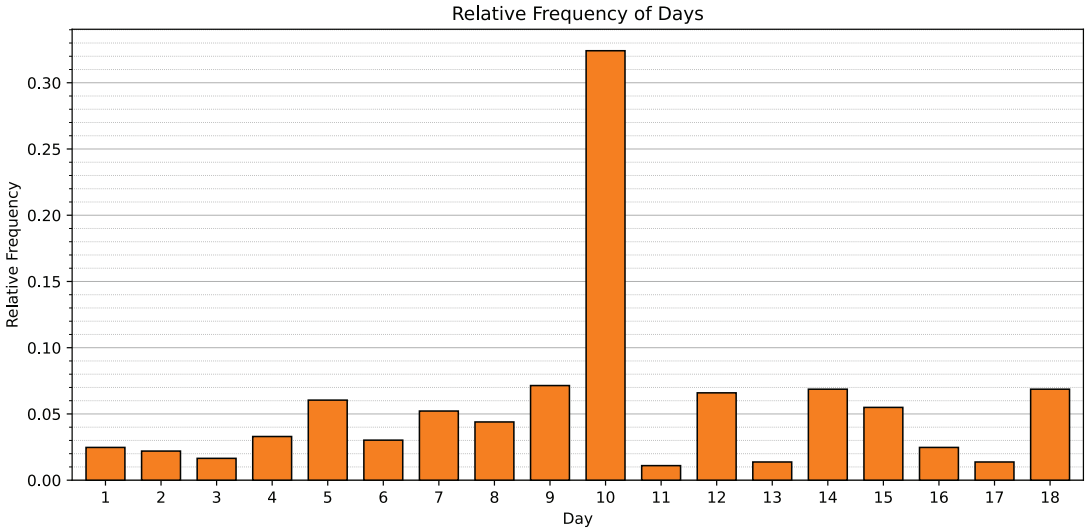

Fig. 7. Relative frequency of the weights for every of the 18 example days for the upscaling to a full year.

resulting system costs C_{syst} of each year t are discounted with the discount rate i (for Germany 2.2% [52]) and added up until the end of the PV system$^{\text{TM}}$s lifetime L_{PV}. Similar to the lifetime costs, the lifetime energy in the denominator is also calculated by discounting and adding up the yearly supplied energy E_{syst} for the entire lifetime. Due to the one-year simulation time frame, E_{syst} does not change and is assumed constant for all years. To scale the 18 example days of year 2020 up to a year, a matching between the classes of each example day and the classes of the days of the year 2020 is performed (Fig. 2). For every day of year 2020, the example day which is most similar (i.e. with the minimum RMSE) is selected. Figure 7 shows the weights for every of the 18 example days for the scaling to a full year. Rather than including artificial penalties for missed ramps, the requirement in this study is to comply with the ramp rate regulations at all time.

5 Results

This section presents the key findings of the study, beginning with a thorough evaluation of the PVPP model's performance based on various error metrics. It then assesses the efficacy of different control strategies in managing energy yield, ramp rates, and battery usage and the results of the economic analysis.

5.1 PVPP model validation

The performance evaluation of the PV model is examined with the following error metrics and shown in Table A.1. Similar to [8], the normalized root mean square error (nRMSE, (15)), the normalized mean average error (nMAE, (16)) and the normalized bias (nBIAS, (17)) quantify the performance of the PV model. The relative values are normalized to the maximum value of the respective day. In the formulas, n is the number of time steps dataset, y_i the validation values, and y_i the P50 lead time 0 predictions.

$$\text{nBias} = \frac{1}{\max(y)} \frac{1}{n} \sum_{i=1}^{n} (\widehat{y}_i - y_i). \tag{15}$$

$$\text{nRMSE} = \frac{1}{\max(y)} \sqrt{\frac{1}{n} \sum_{i=1}^{n} (\widehat{y}_i - y_i)^2}. \tag{16}$$

$$\text{nMAE} = \frac{1}{\max(y)} \frac{1}{n} \sum_{i=1}^{n} |\widehat{y}_i - y_i|. \tag{17}$$

Figure 8 shows the performance of the PVPP model over the 18 days. The error estimation is made with percentile P50 and lead time 0. The nowcasting system was studied by Blum [17] and the estimated RMSE for the deterministic global horizontal irradiation with lead time 0 is $50\,\text{W/m}^2$. In Figure 8, it can be seen that the distributions show a high spread. The values for the nRMSE of each day range from 2.7% to 21.7%. The selected days include a variety of irradiance conditions such as clear-sky days as well as days of highly variable conditions. The performance for these highly variable conditions decreases, whereas the performance increases for days with clear-sky conditions. This is expected since clouds are scarce in clear-sky conditions and abundant in highly variable conditions and determine the uncertainty in nowcasting. The model is positively biased by 0.5%. The limitations of the physical model approach are its complexity, its dependence on various environmental factors, and its dependence on updates to the model in case of changes of the power plant. The physical model is complex and depends on many chained model assumptions leading to limitations of the overall model's accuracy. The model's dependence on environmental factors, e.g.

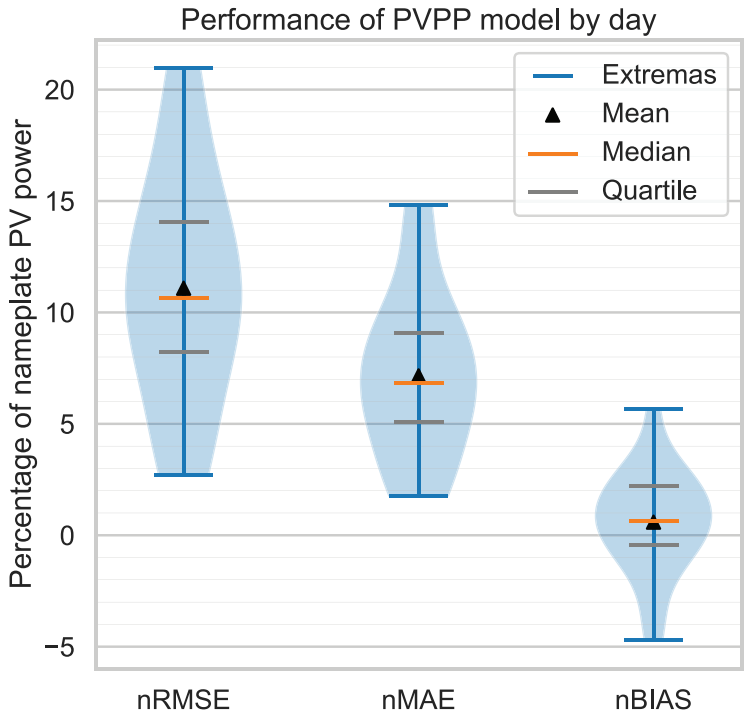

Fig. 8. Distributions of the error metrics nRMSE, nMAE and nBIAS for the 18 days. The error estimation is made with percentile P50 and lead time 0. Metrics are normalized to the maximum of each day.

temperature, windspeed, irradiance, requires extensive data collection of these quantities for improved model performance. Simplifications on the other hand increase the model's ignorance towards changes in these parameters. In case the circumstances of the power plant change, the model needs to be updated to maintain its accuracy. E.g. changes in local shading, soiling of the panels, damaged and replaced components and inhomogeneities within the power plant impact the model's accuracy.

5.2 Control strategy evaluation

Figure 9 shows the performance overview of the control strategy as the cumulative of the 18 days. The first plot shows the respective energy yield of the system. The energy loss of strategy MIX in comparison to strategy VAL is 12.5%. The IDV strategy results in a loss of 1.3% compared to strategy VAL. This is the upper limit for battery-less ramp rate control with ideal nowcasts for these 18 days. The amount of curtailment is dependent on the number of false positive ramp events, e.g. seen in Figure 10 in the morning. Here, two ramps were projected but no ramp occurred in the validation. The opposite case is omitted ramps. The second plot in Figure 9 shows the number of missed ramps. The missed ramps were not correctly predicted from the nowcasts and the battery strategy had to compensate. Of 769 ramps in the dataset, 81.3% or 625 ramps could be prevented by applying the MIX strategy. The IDV strategy shows no ramps, which was expected due to the ideal nowcasts. Hereby, a missed ramp is every timestep, in which the output power gradient, the gradient before battery operation, exceeds the limit. For this case, every small exceedance leads to a count in the missed ramps metric. For the 01.09.2020, small ramp rate violations can be observed. The following plots show the impact of the missed ramps. The maximum ramp depth of these missed ramps is shown in the third plot. Since it is the decisive factor for the required battery power in this study, the reduction of 47.4% is significant. The value for strategy IDV is zero. In this context, a study analysing the penalties is of interest to evaluate further reduction in battery power or battery-less operation, which is not in the scope of this study. The required cumulative discharge energy was reduced by 81.5%, as shown in plot four. Plot five shows the distribution of battery discharge events. The largest discharge was reduced by 48.3%. Discharge events appear less frequent and require less power in strategy MIX then in VAL. Further, the strategy is able to reduce the span between the highest and the lowest state of charge in the dataset from 40.8% for strategy VAL to 11.8% for MIX. This is a reduction of 71.1%. For strategy IDV, the discharge energy is zero, thus no battery is required for compliant operation. The BESS purpose in this study is to step in when the control strategy based on nowcasts fails to comply with the ramp rate regulation. Penalties are not covered in this analysis and provide a different operational case. Here, the compliance with the ramp rate constraint was required. Other services the battery energy storage systems can provide, such as peak shifting, frequency control, and more, are not considered as well as operation during the night.

Figure 10 shows an example day in detail. The output power and its gradient are shown for the 01.09.2020. In each plot, the respective measure is shown for the

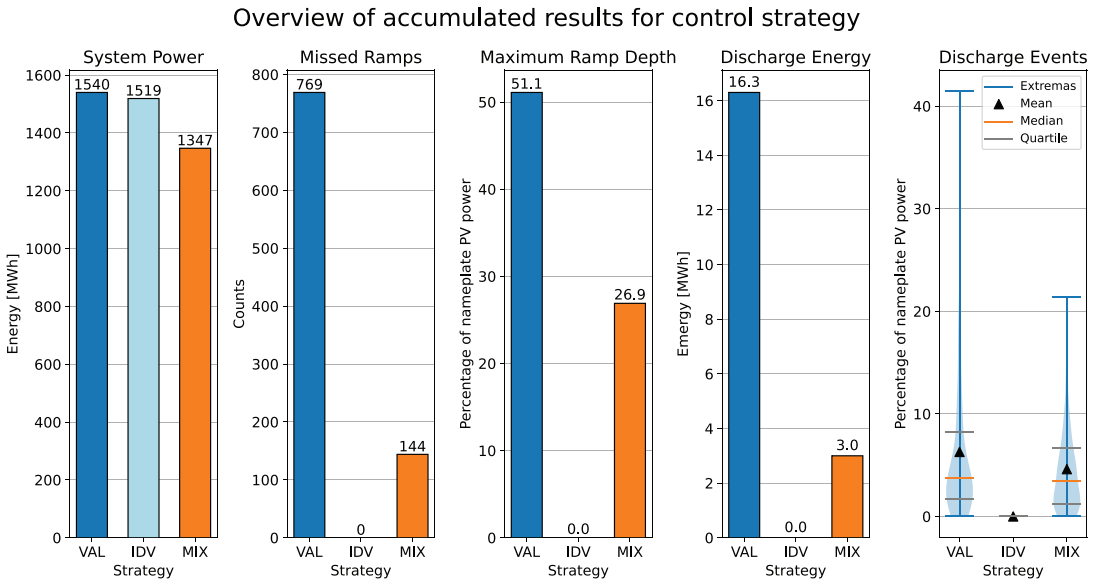

Fig. 9. Performance overview control strategy with strategy MIX in orange, and as reference IDV in light blue and VAL in blue for the 18-day dataset. The first plot shows the respective energy yield. The second and third plots describe the number of ramps and the maximum ramp depth of the missed ramps. Plot four displays the required discharge power of the battery.

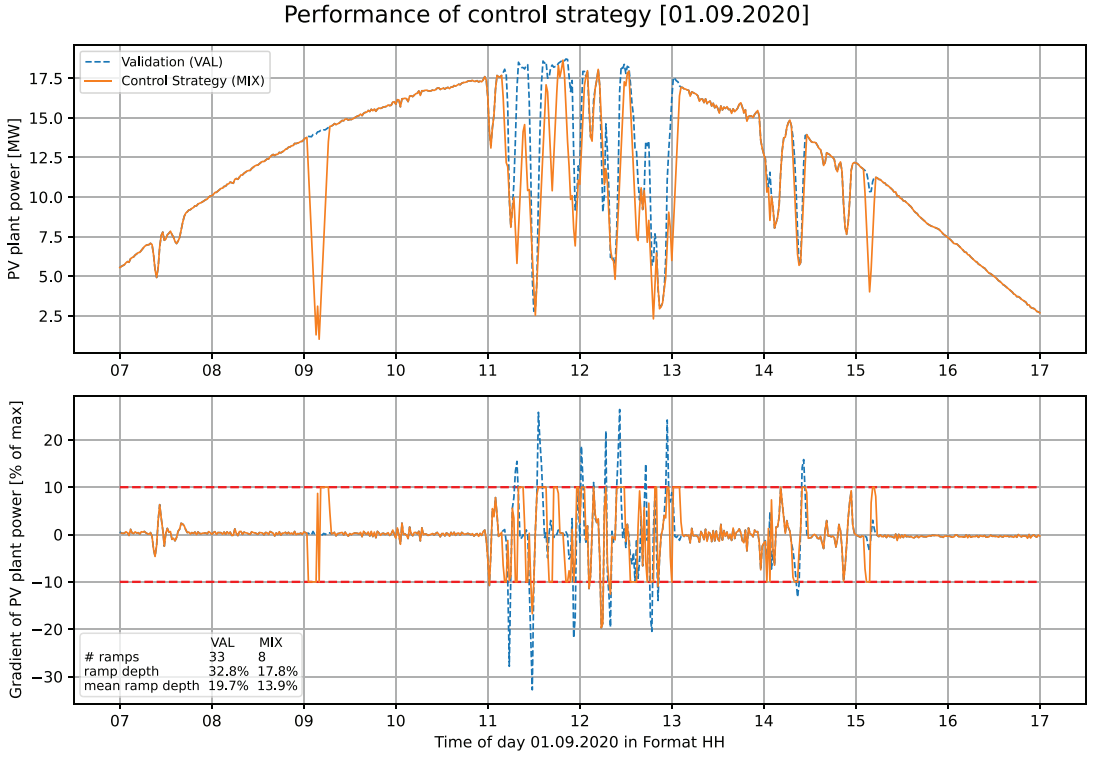

Fig. 10. Output power and its power gradient of the strategies VAL and MIX without battery power for 01.09.2020. The two red dashed lines represent the ramp rate constraint of 10%/min. The text box in the lower left section shows the respective number of remaining ramps, the average, and maximum ramp depth.

validation VAL and control strategy MIX. This day is characterized by mostly clear-sky irradiance conditions except for higher variability at midday. Major events are the false positive ramps at around 09:00, 11:20, 11:45 and 15:10 and large missed ramps at around 11:30 and 12:15. Overall, 33 ramps with an average depth of 17.5% and variability classes of mostly 1 to 4 (almost clear sky to mostly cloudy) were observed. With strategy MIX, the maximum ramp depth is reduced from 32.8% to 19.7%. Eight ramps with an overall average ramp depth of 13.9%

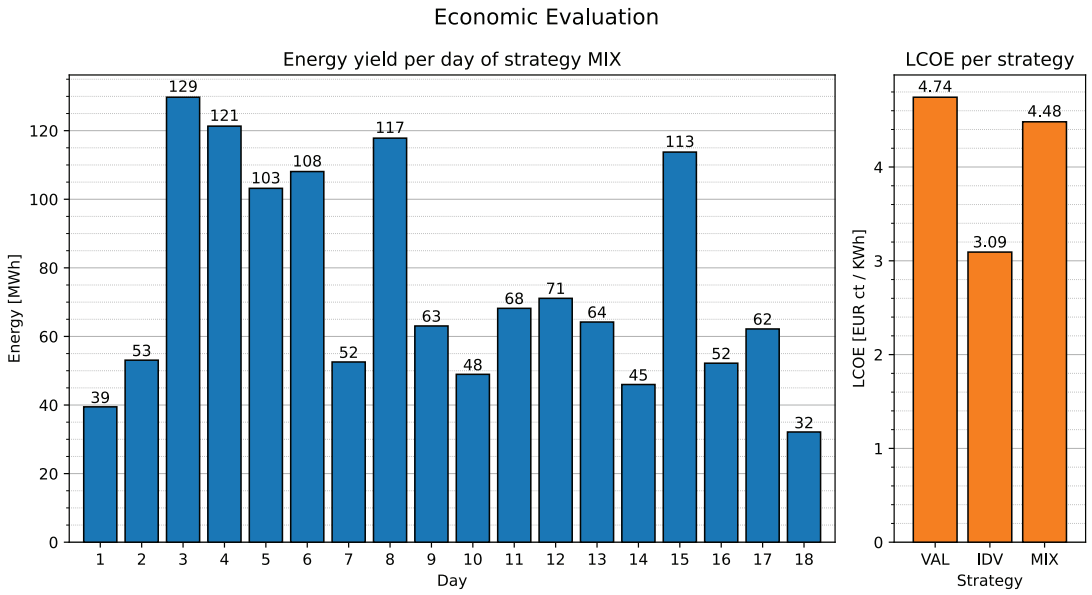

Fig. 11. Economic evaluation results. Left: the energy yield per day of the 18-day dataset for strategy MIX is shown. Right: the LCOEs of the three strategies VAL, IDV and MIX for the upscaled dataset are shown. The lower value for strategy MIX shows the advantage of the proposed Nowcasting system with BESS as backup in this study's economic scenario.

are missed. At 09:00, the strategy leads to a severe ramp-down event although no ramp was observed in the validation data. During high variability conditions of midday, most ramps are detected but the right timing and depth is not always right which leads to the observed gradient exceedances.

The impact of the nowcast uncertainties is quantified by the comparison of the strategy IDV with the strategy MIX. As a result, 81.3% ramps get detected. The remaining ramps required significantly less battery power and capacity to be compensated via a simulated BESS. Further, curtailment due to false positive ramp events is a significant factor for the energy yield of the PVPP, resulting in 12.5% curtailed energy for the 18 day dataset. If compliance with the grid code is required, a BESS is necessary. If compliance is not required but penalties are introduced, the economics depend on their extend, which is not part of this study.

Figure 11 shows the energy yield per day on the left and the LCOEs of the three strategies VAL, IDV and MIX on the right. The LCOEs are scaled up to one year with the weights from Figure 7. The days vary largely in their energy yield. Days with high shares of class one and two result in higher energy yield. Day 10 with a low energy yield of 48 MWh dominates the upscaling due to its relative weight of 32.4%. The energy loss of strategy MIX in comparison to strategy VAL is reduced to 8.7%. The LCOE for strategy IDV is significantly lower (i.e. 34.8%) than for strategy VAL. With strategy IDV, the maximum potential of a control strategy based on nowcasts is estimated. With the conservative assumptions of strategy MIX and existing battery charge rates of 2, a slight reduction in LCOE is achieved, resulting in a large potential for further reduction. The large decrease for IDV can be attributed to the absence of a BESS and to a smaller extend the reduction of curtailment. Strategy MIX is in between with 4.48 EUR ct. This shows the current potential of ramp rate control based on nowcasts in this study's environment. The introduction of penalties would provide an interesting research question for future economic evaluation.

The limitations of the control strategy approach are its dependence on accurate nowcasts, its inability to comply with the ramp rate constraint without a BESS as backup and the share of curtailed energy. The tuning of the control strategy parameters is essential to reduce the number of missed ramps and curtailed energy. Other approaches and parameters within this strategy are recommended to investigate. Hereby, the confidence in each ramp event and the response of the control strategy should be further investigated. It must be taken into account that the used dataset is composed of 18 days, which were chosen because of their particular variability. Yearly figures are expected to be lower due to the strong variability of the selected test days. A further reduction of these figures in a fully realistic case is expected as we assume that the PV system has to be operated without any ramp rate violations, although in reality such exceedances occur together with related economic penalties. To reduce the effect of the selection of test days we scaled up the results of the 18 days to a full year based on irradiance variability classes and evaluated the different PV, battery and nowcasting setups in terms of the Levelized Cost of Electricity (LCOE).

6 Conclusion

In summary, we showed that power smoothing based on nowcasting provides an alternative to battery energy storage systems (BESS) based power smoothing. We demonstrated that nowcasts reduce ramp rate violations, i.e. power gradients larger then allowed by grid codes, by 81.3% and decreases maximum depth by 47.4%. The required battery capacity and maximum power has shown

to be reduced by 71.1% and 48.3%, respectively, at the cost of an estimated 12.5% curtailment loss, i.e. loss through reduction of power, compared to a benchmark without nowcasting. The value for curtailment is reduced to 8.7% in the upscaling to a year, following its dependence on the dataset and PVPP's location. We found that, if compliance with the grid code is maintained, the BESS in combination with nowcasting can be of reduced capacity and power. The economic advantage over the BESS only system, was quantified to 4.48 over 4.74 EUR cents for the LCOE. Hereby, the upscaling for one year was used. The upper limit for nowcasting based output power smoothing is described through strategy ideal validation (IDV), using ideal nowcasts. It was found it has the lowest LCOE in this study of 3.09 EUR cents, showing the potential of improved forecast and control strategy.

The results of our research directly impact the optimization of renewable energy systems. While the current capabilities of nowcasting systems do not completely eliminate the need for battery storage, they do offer the potential for meaningful reductions in both battery capacity and power. Further improvements of nowcasts show a large potential in the reduction of LCOE in this study. This points to a more resource-efficient approach for photovoltaic power plants while alignment with grid codes is required. The nowcasts uncertainties impact the ramp rate control directly through uncertainties in predicted ramp occurrence and depth. This leads to false positive ramps which result in curtailed energy. On the other hand, ramps are still missed. This requires improvements in the nowcasts accuracy and a method to reduce their impact on the control strategy. Hereby, a confidence measure in the predicted ramps could be implemented to reduce the curtailed energy. Future research could study the parameters involved in the control strategy for improving the systems performance on missed ramps and curtailed energy. Specifically mentioned here are the forecast horizon, the selection of percentiles and the confidence in previously detected ramps. Further, the exploration of penalty schemes could advance this study's economic simulations.

Acknowledgments

ChatGPT (GPT-4, OpenAI's large-scale language-generation model) has been used to improve the writing style of this Article. J. Schaible reviewed, edited, and revised the ChatGPT generated texts to his own liking and takes ultimate responsibility for the content of this publication.

Funding

This research was conducted within the DLR institute of Solar Research and received internal funding from the DLR innovation and transfer fund.

J. Schaible thanks the Helmholtz Einstein International Berlin Research School in Data Science (HEIBRiDS) for funding the writing process, which was conducted at the Berlin Joint Lab for Optical Simulations for Energy Research (BerOSE) of Helmholtz-Zentrum Berlin für Materialien und Energie GmbH, Zuse Institute Berlin and Freie Universität Berlin.

Conflicts of interest

The authors have nothing to disclose.

Data availability statement

Data associated with this article cannot be disclosed due to legal reason.

Author contribution statement

J. Schaible, M. Loevenich, N. Blum designed the model and the computational framework. L. Höpken and J. Schaible conducted the economic analysis. J. Stührenberg and A. Hammer developed and provided the nowcasts from the Eye2Sky measurement network. B. Nouri, T. Kotzab and S. Wilbert conceived the study and were in charge of overall direction and planning. J. Schaible wrote the manuscript with input from all authors and support from C. Becker and K. Jäger.

References

1. P.R. Shukla, J. Skea, R. Slade, A. Al Khourdajie, R. van Diemen, D. McCollum, M. Pathak, S. Some, P. Vyas, R. Fradera, M. Belkacemi, A. Hasija, G. Lisboa, S. Luz, J. Malley (eds.), IPCC 2022 summary for policymakers, in *Climate Change 2022: Mitigation of Climate Change*, Contribution of Working Group III to the Sixth Assessment Report of the Intergovernmental Panel on Climate Change, 2022. https://doi.org/10.1017/9781009157926
2. O. Edenhofer, R. Pichs-Madruga, Y. Sokona, K. Seyboth, P. Eickemeier, P. Matschoss, G. Hansen, S. Kadner, S. Schlömer, T. Zwickel, C. Von Stechow, IPCC, 2011 summary for policymakers, in *IPCC Special Report on Renewable Energy Sources and Climate Change Mitigation*, 2011. https://doi.org/10.5860/CHOICE.49-6309
3. E.A. Soto, L.B. Bosman, E. Wollega, W.D. Leon-Salas, Analysis of grid disturbances caused by massive integration of utility level solar power systems, Eng **3**, 236 (2022)
4. REN21, Renewables 2021 Global Status Report, 2021
5. A. Ryu, H. Ishii, Y. Hayashi, Battery smoothing control for photovoltaic system using short-term forecast with total sky images, Electric Power Syst. Res. **190**, 106645 (2021)
6. P. Denholm, R. Margolis, Energy Storage Requirements for Achieving 50% Solar Photovoltaic Energy Penetration in California, Technical Report, 2016
7. A. Makibar, L. Narvarte, E. Lorenzo, Contributions to the size reduction of a battery used for PV power ramp rate control, Solar Energy **230**, 435 (2021)
8. R. Samu, M. Calais, G.M. Shafiullah, M. Moghbel, M.A. Shoeb, B. Nouri, N. Blum, Applications for solar irradiance nowcasting in the control of microgrids: a review, Renewable Sustainable Energy Rev. **147**, 111187 (2021)
9. E. Cirés, J. Marcos, I. de la Parra, M. García, L. Marroyo, The potential of forecasting in reducing the LCOE in PV plants under ramp-rate restrictions, Energy **188**, 116053 (2019)
10. X. Chen, Y. Du, E. Lim, H. Wen, L. Jiang, Sensor network based PV power nowcasting with spatio-temporal preselection for grid-friendly control, Appl. Energy **255**, 113760 (2019)
11. B. Elsinga, W.G.J.H.M. van Sark, Short-term peer-to-peer solar forecasting in a network of photovoltaic systems, Appl. Energy **206**, 1464 (2017)
12. M. Saleh, L. Meek, M.A.S. Masoum, M. Abshar, Battery-less short-term smoothing of photovoltaic generation using sky camera, IEEE Trans. Ind. Informatics **14**, 403 (2018)
13. Q. Paletta, G. Arbod, J. Lasenby, Benchmarking of deep learning irradiance forecasting models from sky images – an in-depth analysis, Solar Energy **224**, 855 (2021)

14. H. Wen, Y. Du, X. Chen, E. Lim, H. Wen, L. Jiang, W. Xiang, Deep learning based multistep solar forecasting for PV ramp-rate control using sky images, IEEE Trans. Ind. Informatics **17**, 1397 (2021)
15. X. Chen, Y. Du, E.G. Lim, L. Fang, K. Yan, Towards the applicability of solar nowcasting: a practice on predictive PV power ramp-rate control, Renewable Energy **195**, 147 (2022)
16. Z. Liu, Y. Du, Evolution towards dispatchable PV using forecasting, storage, and curtailment: a review Electric Power Syst Res. **223**, 109554 (2023)
17. N. Blum, S. Wilbert, B. Nouri, J. Stührenberg, J.E. Lezaca Galeano, T. Schmidt, D. Heinemann, V. Thomas, A. Kazantzidis, R. Pitz-Paal, Analyzing spatial variations of cloud attenuation by a network of all-sky imagers, Remote Sens. **14**, 5685 (2022)
18. N.B. Blum, S. Wilbert, B. Nouri, J. Lezaca, D. Huckebrink, A. Kazantzidis, D. Heinemann, L.F. Zarzalejo, M.J. Jiménez, R. Pitz-Paal, Measurement of diffuse and plane of array irradiance by a combination of a pyranometer and an all-sky imager, Solar Energy **232**, 232 (2022)
19. M. Schroedter-Homscheidt, M. Kosmale, S. Jung, J. Kleissl, Classifying ground-measured 1 minute temporal variability within hourly intervals for direct normal irradiances, Meteorol. Zeitsch. **27,** 161 (2018)
20. B. Nouri, S. Wilbert, L. Segura, P. Kuhn, N. Hanrieder, A. Kazantzidis, T. Schmidt, L. Zarzalejo, P. Blanc, R. Pitz-Paal, Determination of cloud transmittance for all sky imager based solar nowcasting, Solar Energy **181**, 251 (2019)
21. B. Nouri, S. Wilbert, N. Blum, Yann Fabel, E. Lorenz, A. Hammer, T. Schmidt, L. Zarzalejo, R. Pitz-Paal, Probabilistic solar nowcasting based on all-sky imagers, Solar Energy **253**, 285 (2023)
22. B. Nouri, S. Wilbert, P.M. Kuhn, N. Hanrieder, M. Schroedter-Homscheidt, A. Kazantzidis, L.F. Zarzalejo, P. Blanc, S. Kumar, N. Goswami, R. Shankar, R. Shankar, R. Affolter, R. Pitz-Paal, Real-time uncertainty specification of all sky imager derived irradiance nowcasts, Remote Sensing **11**, 1059 (2019)
23. M. Loevenich, L. Kaborn, DLR Internal documentation, YACOP, 2020
24. T. Hirsch, J. Dersch, T. Fluri, J. Garcia-Barberena, S. Giuliano, F. Hustig-Diethlem, R. Meyer, N. Schmidt, M. Seitz, E. Yildiz, SolarPACES guideline for bankable STE yield assessment, IEA-SolarPACES, 2017
25. W.F. Holmgren, C.W. Hansen, M.A. Mikofski, pvlib python: a python package for modeling solar energy systems, J. Open Source Softw. **3**, 884 (2018)
26. W. Holmgren, Calama-Consulting, C. Hansen, K. Anderson, M. Mikofski, A. Lorenzo, U. Krien, bmu, C. Stark, DaCoEx, A. Driesse, A.R. Jensen, M. Sánchez de León Peque, konstantt, mayudong, Heliolytics, Ed Miller, M.A. Anoma, V. Guo, L. Boeman, J. Stein, W. Vining, jforbess, T. Lunel, A. Morgan, J. Ranalli, C. Leroy, A.M.R., J. PalakapillyKWH, J. Dollinger, pvlib/pvlib-python: v 0.9.0 (2021). https://doi.org/10.5281/ZENODO.5366883
27. J.S. Stein, The Photovoltaic Performance Modeling Collaborative (PVPMC) (2012). https://doi.org/10.1109/PVSC.2012.6318225
28. J.J. Michalsky, The Astronomical Almanac's algorithm for approximate solar position (1950−2050), Solar Energy **40**, 227 (1988)
29. B. Nouri, N. Blum, S. Wilbert, L.F. Zarzalejo, A hybrid solar irradiance nowcasting approach: combining all sky imager systems and persistence irradiance models for increased accuracy, Solar RRL **6**, 2100442 (2022)
30. D.L. King, W.E. Boyson, J.A. Kratochvil, Photovoltaic array performance model, Sandia Report No. 2004–3535, 8, 2004
31. N. Blum, Nowcasting of solar irradiance and photovoltaic production using a network of all-sky imagers, PhD thesis, RWTH Aachen, 2022
32. W. De Soto, S.A. Klein, W.A. Beckman, Improvement and validation of a model for photovoltaic array performance, Solar Energy **80**, 78 (2006)
33. A.P. Dobos, P.V. Watts, Version 5 Manual (NREL/TP-6A20- 6264 1), National Renewable Energy Laboratory (NREL), 2014
34. J. Marcos, O. Storkël, L. Marroyo, M. Garcia, E. Lorenzo, Storage requirements for PV power ramp-rate control, Solar Energy **99**, 28 (2014)
35. A. Sangwongwanich, Y. Yang, F. Blaabjerg, A cost-effective power ramp-rate control strategy for single-phase two-stage grid-connected photovoltaic systems, Institute of Electrical and Electronics Engineers Inc., 2016
36. PREPA, Puerto Rico Electric Power Authority minimum technical requirements for photovoltaic (PV) generation projects, 2012
37. X. Li, D. Hui, X. Lai, Battery energy storage station (BESS)-based smoothing control of photovoltaic (PV) and wind power generation fluctuations, IEEE Trans. Sustainable Energy **4**, 464 (2013)
38. L. Höpken, Reducing the Impact of Irradiance Ramps on PV Power Production – A Techno-Economic Analysis of Nowcasting. Master's thesis, RWTH Aachen, 2023
39. V. Ramasamy, J. Zuboy, E. O'Shaughnessy, D. Feldman, J. Desai, M. Woodhouse, P. Basore, R. Margolis, U.S. Solar Photovoltaic System and Energy Storage Cost Benchmarks, With Minimum Sustainable Price Analysis: Q1 2022, 2022. https://doi.org/10.2172/1891204
40. C. Kost, Stromgestehungskosten Erneuerbarer Energien, Fraunhofer-Institut für Solare Energiesysteme ISE, 2021
41. Renewable Power Generation Costs in 2021, International Renewable Energy Agency (IRENA), Abu Dhabi
42. National Renewable Energy Laboratory (NREL), Annual Technology Baseline: Utility-Scale PV, Accessed: 21/08/ 2023. https://atb.nrel.gov/electricity/2022/utility-scale_pv
43. US Dollar (USD) to Euro (EUR) exchange rate history, Accessed: 25/08/2023. https://www.exchangerates.org.uk/USD-EUR-exchange-rate-history.html
44. S.N. Motapon, E. Lachance, L.A. Dessaint, K. Al-Haddad, A generic cycle life model for lithium-ion batteries based on fatigue theory and equivalent cycle counting, IEEE Open J. Ind. Electron. Soc. **1**, 207 (2020)
45. C.S. Lai, Y. Jia, Y. Jia, W. Jia, Z. Xu, L. Lai, X. Li, X. Li, J. Cao, J. Cao, M. McCulloch, Levelized cost of electricity for photovoltaic/biogas power plant hybrid system with electrical energy storage degradation costs, Energy Convers. Manag. **153**, 34–47 (2017)
46. C. Augustine, N. Blair, Storage Futures Study: Storage Technology Modeling Input Data Report, 2021
47. National Renewable Energy Laboratory (NREL), Annual Technology Baseline: Commercial Battery Storage, Accessed: 21/08/2023 https://atb.nrel.gov/electricity/2022/utility-scale_battery_storage
48. National Renewable Energy Laboratory (NREL), Annual Technology Baseline: Utility-Scale Battery Storage, Accessed: 21/08/2023 https://atb.nrel.gov/electricity/2022/commercial_battery_storage
49. European Commission and Directorate-General for Energy and O. Hoogland, V. Fluri, C. Kost, M. Klobasa, M. KÃ¼hnbach, M. Khanra, M. Antretter, J. Koornneef, H. Weijde, A. Satish, E. Battistutta, K. Veum, J. Gorenstein Dedecca, A. Doorman, L. Van Nuffel, B. Breitschopf, A. Herbst, O. Cerny, Study on energy storage, Publications Office of the European Union, 2023, https://doi.org/10.2833/333409
50. Eurostat, Labour cost levels by NACE Rev. 2 activity, Accessed: 21/08/2023 https://ec.europa.eu/eurostat/databrowser/view/lc_lci_lev/default/table?lang=en
51. W. Gerke, M. Bank, *Finanzierung: Grundlagen für Investitions- und Finanzierungs-entscheidungen im Unternehmen* (W. Kohlhammer Verlag, 2016)
52. IRENA, *The cost of financing for renewable power* (International Renewable Energy Agency (IRENA), Abu Dhabi, 2023). https://www.irena.org/Publications/2023/May/The-cost-of-financing-for-renewable-power
53. *National Electricity Rules*. 2023. https://energy-rules.aemc.gov.au/ner/440
54. *National Electricity Amendment (Generator Technical Performance Standards Rule 2018)*. 2018. https://www.aemc.gov.au/rule-changes/generator-technical-performance-standards.
55. *Technical Rules*. 2016. https://www.westernpower.com.au/siteassets/documents/documents-and-policies/technical-rules-20161201.pdf.
56. Horizon Power Technical Rules Standard Number: *HPC-9DJ-01-0001-2012*. 2022. https://web.horizonpower.com.au/media/1287/hpc-9dj-01-0001-2012-horizon-power-technical-rules-nwis-nis-100820.pdf
57. Low Voltage EG Connection Technical Requirements Standard Number:*HPC-9DJ-13-0002-2019*.2021. https://web.horizonpower.com.au/media/5183/low-voltage-eg-connection-technical-requirements.pdf
58. J. Atherton, Rahul Sharma, J. Salgado. Techno-economic analysis of energy storage systems for application in wind farms, Energy **135**, 540 (2017)

59. Regulation FCAS Contribution Factor Procedure. 2023. https://aemo.com.au/-/media/files/electricity/nem/security_and_reliability/ancillary_services/regulation-fcas-contribution-factors-procedure-final.pdf?la=en
60. GB/T 19964-2012 Technical requirements for connecting photovoltaic power station to power system. 2012
61. Technical regulation 3.2.2 for PV power plants above 11 kW. 2016. https://en.energinet.dk/media/evsijtqt/technical-regulation-3_2_2-for-pv-power-plants-above-11-kw.pdf
62. B. Khan, A. Anvari-Moghaddam, J.M. Guerrero, S.K. Chaudhary, J.C. Vasquez, K.H.B. Frederiksen, Y. Wu, A Review of Grid Code Requirements for the Integration of Renewable Energy Sources in Ethiopia, Energies **15**, 5197 (2022). https://doi.org/10.3390/en15145197
63. Technische Anschlussregel Mittelspannung (VDE-AR-N 4110). 2018. https://www.vde-verlag.de/normen/0100495/vde-ar-n-4110-anwendungsregel-2018-11.html
64. *Gesetz für den Ausbau erneuerbarer Energien* (Erneuerbare-Energien-Gesetz- EEG 2023) *§9 Technische Vorgaben*. Accessed: 24/08/2023. https://www.gesetze-im-internet.de/eeg_2014/__9.html
65. V. Gevorgian, S. Booth, Review of PREPA Technical Requirements for Inter connecting Wind and Solar Generation (2013). https://doi.org/10.2172/1260328
66. Central Electricity Authority Notification No.12/X/STD(CONN)/GM/CEA/2018. 2019. https://cea.nic.in/wp-content/uploads/2020/02/notified_regulations.pdf
67. EirGrid Grid Code Version 11. 2022. https://www.eirgridgroup.com/site-files/library/EirGrid/GridCode.pdf
68. R. Khan, Y. Go, Y. Ii Go, Assessment of Malaysia's Large-Scale Solar Projects: Power System Analysis for Solar PV Grid Integration, in: *Global Challenges* (2020), p. 1900060. https://doi.org/10.1002/gch2.201900060
69. *Guidelines On Large Scale Solar Photovoltaic Plant For Connection To Electricity Net works [Electricity Supply Act (Amendment) 2015 (Act A1501)*]. 2018. https://www.st.gov.my/contents/2019/LSS/Guideline%20on%20LSSPV%20for%20Connection%20to%20Electricity%20Networks_%20February%202019.PDF
70. Minimum Technical Requirements for Interconnection of Photovoltaic (PV) Facilities 2012. https://www.esig.energy/wiki-main-page/puerto-rico-electric-power-authority-s-minimum-technical-renewables-interconnection-requirements/#Minimum_Technical_Requirements_of_Interconnection_of_PV_Facilities_.28ver.June_14.2C_2012.29.
71. A. Makibar, A. Makibar, L. Narvarte, E. Lorenzo, On the relation between battery size and PV power ramp rate limitation, Solar Energy **142**, 182 (2017)

Appendix A: Performance error metrics

Table A.1. Error metrics root mean square error, mean absolute error, and bias for all days of the 18-day dataset and cumulative. All three metrics include the absolute (abs.) values [KWh] and relative to max of the respective day [%]. Further, the values for percentile P50 are given. All days are included individually.

		RMSE		MAE		BIAS	
Day	Strategy	Abs	Max	Abs	Max	Abs	Max
All days	P50	2262	12.0	1291	6.9	95	0.5
Median	P50	1984	10.7	1253	6.9	122	0.7
Mean	P50	2067	11.3	1305	7.1	108	0.6
Min	P50	508	2.7	322	1.7	−858	−4.7
Max	P50	4057	21.7	2673	14.3	1057	5.7
2020-03-09	P50	4057	21.7	2673	14.3	1057	5.7
2020-03-16	P50	1948	10.4	1180	6.3	−35	−0.2
2020-03-22	P50	970	5.2	442	2.3	52	0.3
2020-04-11	P50	515	2.9	379	2.1	−93	−0.5
2020-04-12	P50	2614	14.4	1684	9.3	−858	−4.7
2020-04-24	P50	508	2.7	322	1.7	38	0.2
2020-06-07	P50	2666	14.2	1629	8.7	246	1.3
2020-06-17	P50	1872	10.4	1208	6.7	−220	−1.2
2020-06-27	P50	2884	15.8	1687	9.2	−610	−3.3
2020-07-10	P50	2090	11.3	1298	7.0	456	2.5
2020-07-20	P50	2603	13.9	1806	9.7	487	2.6
2020-07-21	P50	3196	17.1	2025	10.8	472	2.5
2020-08-01	P50	1408	8.1	864	5.0	243	1.4
2020-08-23	P50	2021	11.0	1325	7.2	192	1.0
2020-09-01	P50	1039	5.5	559	3.0	−263	−1.4
2020-09-04	P50	3693	20.2	2617	14.3	528	2.9
2020-09-25	P50	1708	9.1	1054	5.6	35	0.2
2020-10-05	P50	1409	9.1	748	4.9	212	1.4

Cite this article as: Jonas Schaible, Bijan Nouri, Lars Höpken, Tim Kotzab, Matthias Loevenich, Niklas Blum, Annette Hammer, Jonas Stührenberg, Klaus Jäger, Christiane Becker, Stefan Wilbert, Application of nowcasting to reduce the impact of irradiance ramps on PV power plants, EPJ Photovoltaics 15, 15 (2024)